Formation of semiconductor vertical quantum barriers by epitaxial growth on corrugated surfaces

G. Biasiol,* K. Leifer, and E. Kapon
Department of Physics, Swiss Federal Institute of Technology Lausanne, CH-1015 Lausanne EPFL, Switzerland
(Received 23 July 1999)

The relationship between growth rate anisotropy, capillarity and entropy of mixing effects, and self-ordering of semiconductor alloy nanostructures grown on nonplanar surfaces, is investigated theoretically and experimentally. It is shown that self-ordered nanostructures enriched by one component of the alloy or the other are formed, depending on the sign of the surface curvature and the growth rate anisotropy. The formation of Al-rich $Al_xGa_{1-x}As$ vertical quantum barriers on convex surfaces with a particular sign of the growth rate anisotropy is experimentally demonstrated.

Lateral self ordering of surface and interface structures provides an attractive means for producing ordered nanostructures of prescribed configuration and composition.[1] The resulting self-ordered nanostructures are essential for studies of low-dimensional quantum structures such as quantum wires[2] (QWR's) and quantum dots (QD's).[3,4] Moreover, their exact form, arrangement and interface quality determine their usefulness in various applications, particularly in electronic and optical semiconductor devices.

Lateral self-ordering mechanisms rely on the movement of atoms and larger atomic complexes on the surface, e.g., during the epitaxial growth of a crystal.[4,5] This movement is driven by gradients of the surface chemical potential,[6] which add surface flux components to the source fluxes arriving from the exterior of the growing surface. The corresponding lateral variations in the surface chemical potential can have various origins, e.g., strain fields,[7] nonplanar surface profiles[8] and nonuniform alloy composition.[9] In the case of self ordering of lateral nanostructures during epitaxial growth of semiconductor compounds, these sources of chemical potential gradients can be introduced via lattice mismatch of the grown layers,[4] nonplanar surface structuring,[5] and preferential alloy segregation at specific crystal facets,[5] respectively. Often, all these effects play in unison to determine the lateral atomic fluxes and hence the resulting lateral nanostructure. For example, in the case of Stranski-Krastanow (SK) growth of $In_xGa_{1-x}As$/GaAs QD's on GaAs substrates,[3,4] strain effects give rise to the formation of lens-shaped islands, which render the surface nonplanar. This nonplanarity introduces capillarity surface fluxes, which may modify the form of the resulting island as compared with what is expected on the basis of strain fields alone. Furthermore, the ordered vertical stacking of SK dots, which has been explained as due to residual strain fields above a given island,[4] could also be affected by the nonplanarity of the surface. Finally, In segregation at the $In_xGa_{1-x}As$ islands[10,11] will alter the surface fluxes via the entropy of mixing term in the surface chemical potential. A detailed understanding of the interplay of these mechanisms is thus necessary in order to predict and control the lateral ordering and the potential wells of the resulting low-dimensional nanostructures.

In the present work, we address the interplay of surface curvature and alloy segregation in the self-formation of lateral nanostructures in $Al_xGa_{1-x}As$ layers grown on corrugated GaAs/$Al_xGa_{1-x}As$ surfaces. Specifically, we show that the sign of the growth rate anisotropy and the surface curvature determine whether a convex or a concave self-limiting surface nanostructure develops. Furthermore, we show that alloy segregation on such self-limiting curved surfaces with either poor or rich content of the fast-diffusing group-III species results, depending on the nature of the surface curvature. The formation of Al-rich vertical quantum barriers (VQB's) on self-limiting, nm-sized ridges is observed and explained using the above mentioned mechanisms.

We consider the surface evolution of an alloy during lattice-matched epitaxial growth, therefore neglecting strain effects. Any changes of orientation or composition on the surface show up as variations in the surface chemical potential μ. For a surface profile faceted along one direction (see Fig. 1), the chemical potential on a facet i, surrounded by two sidewalls s misoriented by the same angle θ with respect to the horizontal, can be written (for a component with mole fraction x_i) as[5]

$$\mu_i = \mu_0 \pm \gamma\Omega_0 / l_i + k_B T \ln x_i , \tag{1}$$

where μ_0 is the chemical potential for a uniform surface, the second term is due to surface nonplanarity (capillarity), and the third is due to the entropy of mixing. In this equation, $\gamma = 2(\gamma_s \csc\theta - \gamma_i \cot\theta)$, γ_s and γ_i are the surface free energy of the sidewalls and of facet i, respectively, Ω_0 is the atomic volume, l_i is the width of facet i, and the signs $-$ and $+$ refer to a concave and convex profile, respectively. The capillarity term reflects the lowering of μ at a concave surface,[6] while the entropy of mixing term expresses the tendency toward a uniform composition (i.e., maximum disorder).[9]

For a binary compound like GaAs or AlAs, the composition is uniform throughout the surface, thus only capillarity effects are present. Through the Nernst-Einstein equation, one can calculate from Eq. (1) the diffusion fluxes at a concave or a convex profile like the ones shown in Figs. (1)(a) and (1)(b), respectively. Such profiles are a simplified picture of those occurring, for example, at the bottom and at the top of a periodic *V*-grooved corrugation. Assuming that these

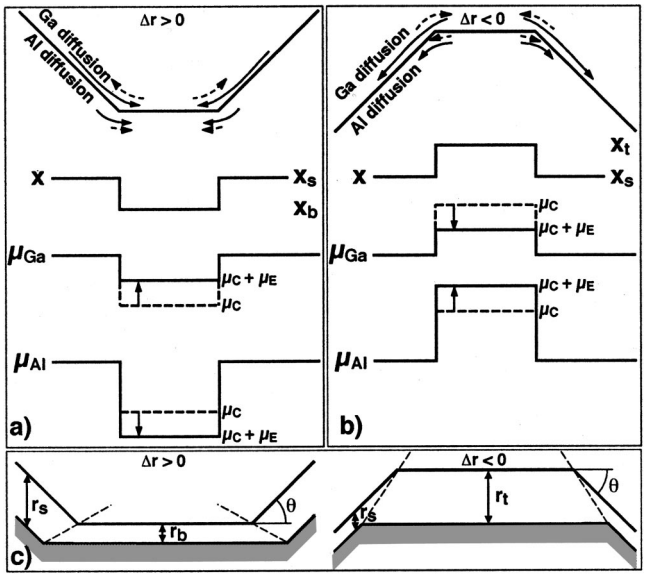

FIG. 1. (a) from top to bottom: schematics of a concave profile, with direction and relative magnitude of capillarity (solid arrows) and entropy-related (dashed arrows) fluxes, for Ga and Al; composition profile; profiles of the Ga and Al chemical potentials (dashed line: capillarity contribution, solid line: with entropy of mixing correction). (b) The same at a convex profile. (c) Schematics of the narrowing of a concave (left) and convex profile (right).

profiles are composed of a single bottom (label b) or top (t) facet, with the same orientation (and hence $\gamma_b=\gamma_t$), and surrounded by a sidewall (s), the capillarity fluxes are written:

$$j_b^C=+\frac{r_s L_s^2 \gamma}{k_B T l_b^2}, \quad j_t^C=-\frac{r_s L_s^2 \gamma}{k_B T l_t^2}, \tag{2}$$

where r_s is the ''intrinsic'' growth rate on the sidewalls (i.e., the growth rate due to deposition, in the absence of capillarity fluxes) and L_s is the sidewall diffusion length. The ''+'' sign in Eq. (2) indicates diffusion from the sidewalls to the bottom region, while the ''−'' sign indicates diffusion from the top region to the sidewalls. Thus, the intrinsic growth rates r_b and r_t at the bottom and at the top are respectively increased and decreased by capillarity.[12]

Capillarity fluxes (2) become high enough to alter significantly the bottom and top growth rates only when these regions narrow down to sizes in the 10-nm range. To reach these sizes starting from an arbitrarily wide bottom or top profile, the intrinsic growth rates at these regions must be smaller (bottom) or larger (top) than r_s. This situation is shown schematically in Fig. 1(c), where Δr denotes the intrinsic growth rate anisotropy, defined as $\Delta r=r_s-r_b$ at the bottom, and $\Delta r=r_s-r_t$ at the top. The establishment of a stable set of facets with the suitable Δr depends in a complex way on the shape of the initial patterned substrate, on the growth technique and parameters, on the materials and on the surface morphology.[13,14] In the present study we will not consider the origin of the anisotropy, but rather concentrate on its effects on self ordering.

If $\Delta r>0$ at the bottom and $\Delta r<0$ at the top, capillarity fluxes can completely compensate for the intrinsic growth rate anisotropy. Beyond this point, the groove or ridge will further evolve by keeping a constant width. This *self-limiting* width of the bottom (l_b^{sl}) or top regions (l_t^{sl}) can be expressed analytically for binary compounds (e.g., GaAs or AlAs) as[5]

$$l_b^{sl}=\left(C\frac{r_s}{\Delta r}\right)^{1/3} \quad (\Delta r>0)$$

$$l_t^{sl}=\left(C\frac{r_s}{-\Delta r}\right)^{1/3} \quad (\Delta r<0),$$

where $C=2\Omega_0 L_s^2\gamma/k_BT$. Note that a self-limiting bottom (top) can develop only if $\Delta r>0(\Delta r<0)$, otherwise the expressions above are meaningless.

For an $Al_xGa_{1-x}As$ alloy, the dependence of the capillarity fluxes (2) on the adatom diffusion length produces a region rich in the fast-diffusing species (i.e., Ga) at the bottom, and in the slow-diffusing ones (Al) at the top (see composition profiles in Fig. 1). These segregated regions give rise to a bottom vertical quantum well[15–17] (VQW) and, as we will show here, a top VQB, respectively. However, capillarity-induced segregation is partly hindered by entropy of mixing effects [Eq. (1)]. At the Ga-rich bottom ($x_b<x$), these effects tend to raise μ_{Ga} and to lower μ_{Al}, while the opposite happens at the Al-rich top ($x_t>x$), as shown in Figs. 1(a) and 1(b), respectively. These effects can be incorporated into the Nernst-Einstein equations by adding the entropy-related term to μ_{Ga} and μ_{Al}.[5] The resulting, additional surface fluxes j^E are

$$j_b^{E,A}=\frac{r_s(L_s^A)^2}{\Omega_0 l_b}\ln\frac{x}{x_b}>0, \quad j_b^{E,G}=\frac{r_s(L_s^G)^2}{\Omega_0 l_b}\ln\frac{1-x}{1-x_b}<0,$$

$$j_t^{E,A}=\frac{r_s(L_s^A)^2}{\Omega_0 l_t}\ln\frac{x}{x_t}<0, \quad j_t^{E,G}=\frac{r_s(L_s^G)^2}{\Omega_0 l_t}\ln\frac{1-x}{1-x_t}>0,$$

where the indexes A and G refer to AlAs and GaAs, respectively. The direction and relative magnitude of entropy-related fluxes are shown with dashed arrows in Figs. 1(a) and 1(b). Note the different combination of capillarity and entropy-related Ga and Al fluxes at the bottom and at the top.

From the discussion above, one can conclude that the intrinsic asymmetry between the self-limiting profiles forming in the concave bottom region and in the convex top one, are due to the different combinations of capillarity and growth rate anisotropy between these two regions, modified by entropy of mixing effects. This asymmetry manifests itself not only in terms of composition, but also in the way self-limiting profiles are reached. At both regions, profiles widen as the composition of the faster-diffusing material increases and vice versa. However, at the concave region, transients to wider profiles are characterized by an *increase* of the growth rate in the region, while at the bottom they are brought about by a *decrease* of the growth rate.[18] This is because the increase in capillarity fluxes, as surface diffusion increases, determines stronger diffusion fluxes *towards the concave* region, and *away from the convex* one.

Self-limiting $Al_xGa_{1-x}As$ top VQB's and bottom VQW's can be formed *simultaneously*, under appropriate conditions, by organometallic chemical vapor deposition (OMCVD)

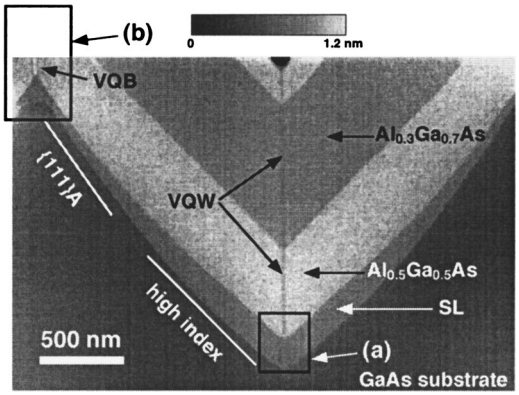

FIG. 2. AFM cross section of a 3 μm-pitch GaAs *V* groove, on which a multilayer $Al_xGa_{1-x}As$ heterostructure was grown. Formations of a bottom-VQW and of a ridge-VQB are indicated.

growth on GaAs (100) substrates patterned with $[01\bar{1}]$-oriented *V* grooves. Figure 2 is an atomic force microscopy (AFM) cross section[19] of part of a 3 μm-pitch *V* groove, on which a multilayer $Al_xGa_{1-x}As$ structure was grown at 700 °C by low-pressure OMCVD (growth parameters are reported elsewhere[20]). The structure consists of a nominally 600 nm-thick $Al_{0.3}Ga_{0.7}As$ layer, sandwiched between a 400 nm- and a 130 nm-thick $Al_{0.5}Ga_{0.5}As$ barriers. A short-period $GaAs/Al_{0.5}Ga_{0.5}As$ superlattice (SL) buffer was grown before the $Al_xGa_{1-x}As$ structure. At the bottom of the groove, a darker vertical stripe evidences the formation of a Ga-rich, self-limiting VQW,[17] throughout all the $Al_xGa_{1-x}As$ layers. Similarly, also the region at the top of the mesa sharpens up during SL growth (top left of the image). Eventually, it reaches a self-limiting width in the $Al_xGa_{1-x}As$ layer, where a brighter vertical stripe is visible, indicating an Al-rich VQB.

The details at the bottom and top regions (framed regions in Fig. 2) are better imaged in the transmission electron microscopy (TEM) cross sections of Fig. 3. At the bottom of the groove (a), the SL layers can now be clearly resolved, and allow the distinction of a central (100) facet, separated from the sidewalls by two {311} *A* ones (see dashed lines).[21] One can also notice a thickening of the GaAs layers and a Ga enrichment in the $Al_{0.5}Ga_{0.5}As$ ones, with respect to the sidewalls.[21] The bottom of the groove narrows down from

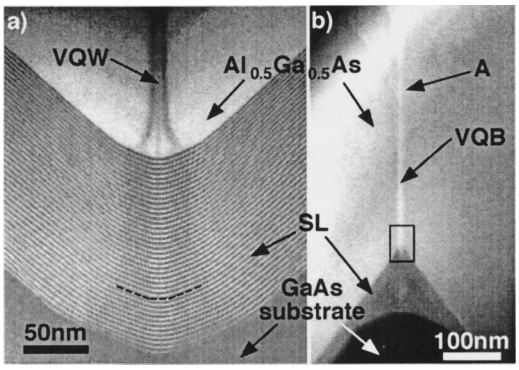

FIG. 3. Dark-field TEM cross sections showing the SL and the beginning of the $Al_{0.5}Ga_{0.5}As$ layer from the structure of Fig. 2 (framed rectangles). (a): Detail at the bottom of the groove. (b): Detail at the top of the ridge.

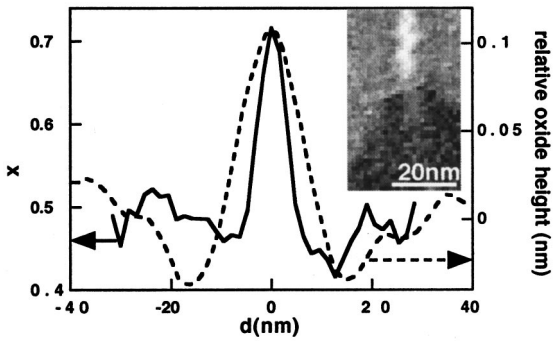

FIG. 4. Inset: Cross-sectional EELS composition map of the VQB region from Fig. 3(b) (framed rectangle). Solid line: EELS line scan across the VQB . Dashed line: AFM line scan of the same region, showing oxide heights on an air-exposed cross section.

the etched substrate and stabilizes to about 50-nm width in the SL region after a thickness of ~ 50 nm. It narrows down again to a new self-limiting width of about 15 nm in the $Al_{0.5}Ga_{0.5}As$ region, where three VQW branches, corresponding to the three bottom facets, are clearly resolved.[17]

The corresponding behavior at the top of the mesa (b) presents some similarities, but also some important differences. The etched profile narrows down also in this case during SL and $Al_{0.5}Ga_{0.5}As$ growth, to a self-limiting width of about 10 nm in this latter layer. The Al-rich VQB forms in the $Al_{0.5}Ga_{0.5}As$ layer, but no branching structure is visible. The self-limiting VQB growth proceeds in the $Al_{0.5}Ga_{0.5}As$ layer, but stops at the point marked with an ''*A*'' in the image. During further growth, the top profile broadens and the compositional contrast smears out.

To quantitatively measure the local VQB composition, we have performed cross-sectional electron energy loss spectroscopy (EELS) measurements.[22] The inset of Fig. 4 shows an EELS compositional map of the VQB region shown in a frame in Fig. 3(b). Both the SL and the $Al_{0.5}Ga_{0.5}As$ layers are visible. The VQB extends in the $Al_{0.5}Ga_{0.5}As$ layer, and also partially in the SL, starting at the point where a self-limiting profile has been reached. The solid line in Fig. 4 shows an EELS line scan across the VQB taken from the inset, and averaged across a vertical region of 15 nm to reduce the scanning noise. The maximum Al concentration x_t at the center of the VQB is about 0.71, that is about 0.2 higher than on the surrounding sidewalls, where the same composition as the nominal one was measured.

The composition profile of $GaAs/Al_xGa_{1-x}As$ heterostructures can be measured as well by cross-sectional AFM in air, via a suitable calibration of the oxide height on the cleaved edge of the samples.[19] The dashed line in Fig. 4 is an AFM line scan across the VQB region from the image shown in Fig. 2, averaged over a 100 nm-thick region. Note that the VQB appears broader than in the EELS scan, possibly due to the lower spatial resolution of cross-sectional AFM, as compared to EELS, and to lateral growth of the oxide layer above the VQB. The maximum height difference between the VQB and the surrounding barriers is about 0.11 nm. By assuming a composition $x=0.5$ in the sidewall region and calibrating the oxide height profile in the VQB with the method given in Ref. 19, we obtain $x_t=0.69\pm0.03$, in agreement with the EELS estimate. Note that both EELS and

AFM scans show a region of slightly enhanced (about 0.05 in composition) Ga concentration, extending for about 10 nm on both sides of the VQB, and probably due to Ga segregation at the interface between the top and sidewall planes.

It is important to understand under which conditions a bottom-VQW and a top-VQB can form *simultaneously*. If the bottom and top regions have the same orientation and the sidewalls are composed of a single, straight facet, one can have either $\Delta r>0$ (self-limiting growth at a concave surface) or $\Delta r<0$ (self-limiting growth at a convex surface), depending on the growth technique, growth conditions and orientation of the grooves.[5,18] In our samples, however, the sidewalls of the etched profile consist of an *exactly* oriented $\{111\}A$ facet near the top of the mesas, smoothly connected to a high-index facet near the bottom of the groove, that forms an angle of about 45° with the (100) plane (see Fig. 2). Since the top and bottom regions grow much faster than the $\{111\}A$ facets, but more slowly than the high-index ones,[14] a self-limiting VQB can form at the top, while a self-limiting VQW forms at the bottom. However, the high-index planes consume the $\{111\}A$ ones (Fig. 2), and reach the top of the mesas at point ''*A*'' in Fig. 3(b), after which Δr is reversed in this region. During further growth, the top starts to expand, and the compositional contrast smears out.

In conclusion, we have shown that self ordering of alloys during epitaxial growth on corrugated profiles can be interpreted as due to an interplay among effects of growth rate anisotropy, capillarity and entropy of mixing. The different combination of these three factors, depending on the surface curvature, gives rise to intrinsic asymmetries between concave and convex corners, in terms of composition and transient evolution towards self-limiting profiles. A more complete model, taking into account also the dominant contribution of strain to the surface chemical potential, could be applied to explain self ordering during SK growth of lattice-mismatched alloy QD's,[10,11] in terms of size, vertical correlation and composition. Besides, such strain contribution is needed in order to model self ordering of $In_xGa_{1-x}As/GaAs$ QWR's on nonplanar substrates, where gradients of surface curvature, composition[22] and strain[23] coexist. The VQB structures demonstrated could be useful for studies of tunneling through thin barriers embedded in alloy semiconductor heterostructures.

This work was partially supported by the Fonds National Suisse de la Recherche Scientifique.

*Present address: Laboratorio TASC-INFM, Area Science Park, S.S. 14, Km. 163.5 Basovizza, I-34012 Trieste, Italy.

[1] E. Kapon, Semicond. Semimet. **40**, 259 (1994).
[2] E. Kapon, D.M. Hwang, and R. Bhat, Phys. Rev. Lett. **63**, 430 (1989).
[3] H. Drexler *et al.*, Phys. Rev. Lett. **73**, 2252 (1994).
[4] Q. Xie, A. Madhukar, P. Chen, and N.P. Kobayashi, Phys. Rev. Lett. **75**, 2542 (1995).
[5] G. Biasiol and E. Kapon, Phys. Rev. Lett. **81**, 2962 (1998).
[6] A. Pimpinelli and J. Villain, *Physics of Crystal Growth* (Cambridge University Press, Cambridge, 1998).
[7] D.J. Srolovitz, Acta Metall. **37**, 621 (1989).
[8] W.W. Mullins, J. Appl. Phys. **28**, 333 (1957).
[9] J.Y. Tsao, *Material Fundamentals of Molecular Beam Epitaxy* (Academic Press, Boston, 1993).
[10] A. Krost *et al.*, Appl. Phys. Lett. **68**, 785 (1996).
[11] N. Grandjean, J. Massies, and O. Tottereau, Phys. Rev. B **55**, R10 189 (1997).
[12] We will refer conventionally to growth rates measured along the growth direction. Note that $r_t=r_b$ since they have the same crystallographic orientation.
[13] S. Koshiba *et al.*, J. Appl. Phys. **76**, 4138 (1994).
[14] S.H. Jones, L.S. Salinas, J.R. Jones, and K. Mayer, J. Electron. Mater. **24**, 5 (1995).
[15] M. Walther *et al.*, Appl. Phys. Lett. **60**, 521 (1992).
[16] G. Vermeire *et al.*, J. Cryst. Growth **124**, 513 (1992).
[17] G. Biasiol *et al.*, Appl. Phys. Lett. **69**, 2710 (1996).
[18] G. Biasiol and E. Kapon, J. Cryst. Growth **201-202**, 62 (1999).
[19] F. Reinhardt, B. Dwir, G. Biasiol, and E. Kapon, Appl. Surf. Sci. **104**, 529 (1996).
[20] A. Gustafsson, F. Reinhardt, G. Biasiol, and E. Kapon, Appl. Phys. Lett. **67**, 3673 (1995).
[21] G. Biasiol, E. Kapon, Y. Ducommun, and A. Gustafsson, Phys. Rev. B **57**, R9416 (1998).
[22] K. Leifer *et al.* (unpublished).
[23] M. Grundmann, O. Stier, and D. Bimberg, Phys. Rev. B **50**, 14 187 (1994).